Article

Cell Reports

RNF20 Links Histone H2B Ubiquitylation with Inflammation and Inflammation-Associated Cancer

Graphical Abstract

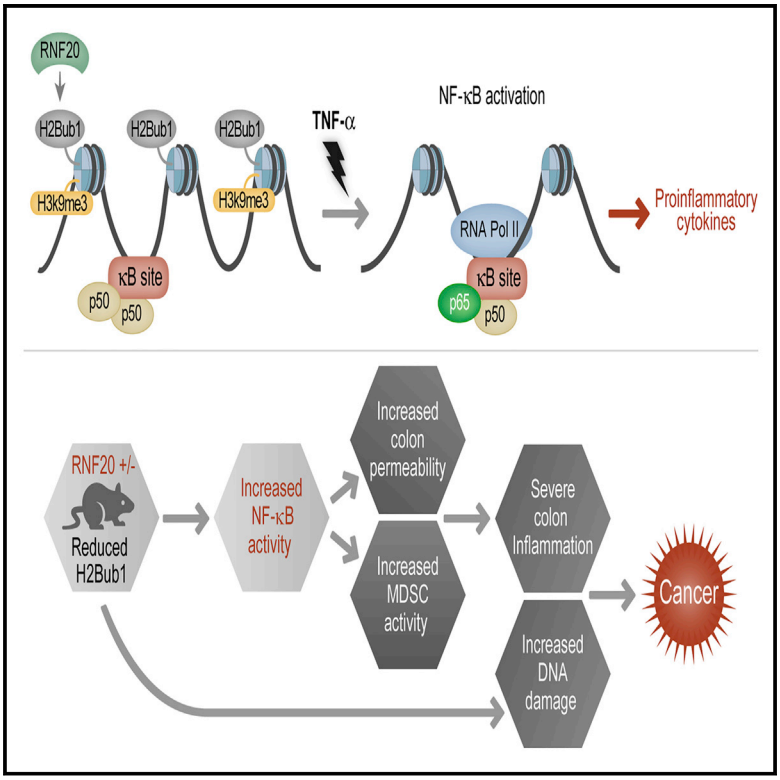

Highlights

- RNF20 and H2Bub1 modulate the NF-kB response
- RNF20-deficient mice are prone to colonic inflammation and colorectal cancer
- Reduced H2Bub1 may create a pro-tumoral microenvironment
- Reduced H2Bub1 is associated with colitis and colorectal cancer in humans

Authors

Ohad Tarcic, Ioannis S. Pateras, Tomer Cooks, ..., Eli Pikarsky, Vassilis G. Gorgoulis, Moshe Oren

Correspondence

moshe.oren@weizmann.ac.il

In Brief

Ubiquitination of histone H2B (H2Bub1), primarily by the E3 ligase RNF20, is reduced in many advanced cancers. Tarcic et al. report that downregulation of RNF20 and H2Bub1 promotes chronic colonic inflammation and inflammation-associated colorectal cancer in mice and humans, partly by augmenting NF-kB activity and attenuating the antitumoral T cell response.

Tarcic et al., 2016, Cell Reports *14*, 1462–1476
February 16, 2016 ©2016 The Authors
http://dx.doi.org/10.1016/j.celrep.2016.01.020

OPEN ACCESS
CellPress

Cell Reports
Article

RNF20 Links Histone H2B Ubiquitylation with Inflammation and Inflammation-Associated Cancer

Ohad Tarcic,[1] Ioannis S. Pateras,[2] Tomer Cooks,[1] Efrat Shema,[1] Julia Kanterman,[3] Hadas Ashkenazi,[3] Hana Boocholez,[3] Ayala Hubert,[4] Ron Rotkopf,[5] Michal Baniyash,[3] Eli Pikarsky,[6,7] Vassilis G. Gorgoulis,[2,8,9] and Moshe Oren[1,*]

[1]Department of Molecular Cell Biology, The Weizmann Institute, Rehovot 7610001, Israel
[2]Molecular Carcinogenesis Group, Department of Histology-Embryology, School of Medicine, University of Athens, 11527 Athens, Greece
[3]The Lautenberg Center for General and Tumor Immunology, Israel-Canada Medical Research Institute, Faculty of Medicine, The Hebrew University, Jerusalem 91120, Israel
[4]Sharett Institute of Oncology, Hebrew University-Hadassah Medical Center, Jerusalem 91120, Israel
[5]Department of Biological Services, Weizmann Institute of Science, Rehovot 7610001, Israel
[6]Department of Immunology and Cancer Research
[7]Department of Pathology
Hebrew University-Hadassah Medical School, Jerusalem 91120, Israel
[8]Biomedical Research Foundation, Academy of Athens, 11527 Athens, Greece
[9]Faculty Institute for Cancer Sciences, University of Manchester, Manchester Academic Health Science Centre, Manchester M13 9WL, UK
*Correspondence: moshe.oren@weizmann.ac.il
http://dx.doi.org/10.1016/j.celrep.2016.01.020

SUMMARY

Factors linking inflammation and cancer are of great interest. We now report that the chromatin-targeting E3 ubiquitin ligase RNF20/RNF40, driving histone H2B monoubiquitylation (H2Bub1), modulates inflammation and inflammation-associated cancer in mice and humans. Downregulation of RNF20 and H2Bub1 favors recruitment of p65-containing nuclear factor κB (NF-κB) dimers over repressive p50 homodimers and decreases the heterochromatin mark H3K9me3 on a subset of NF-κB target genes to augment their transcription. Concordantly, RNF20$^{+/-}$ mice are predisposed to acute and chronic colonic inflammation and inflammation-associated colorectal cancer, with excessive myeloid-derived suppressor cells (MDSCs) that may quench antitumoral T cell activity. Notably, colons of human ulcerative colitis patients, as well as colorectal tumors, reveal downregulation of RNF20/RNF40 and H2Bub1 in both epithelium and stroma, supporting the clinical relevance of our tissue culture and mouse model findings.

INTRODUCTION

Inflammation is a crucial protective response conserved in all multicellular organisms (Medzhitov, 2010). It entails activation of many cell types through several signaling pathways including nuclear factor kappa B (NF-κB) and signal transducer and activator of transcription 3 (STAT3), resulting in release of cytokines and chemokines. Inflammation is tightly regulated and is effectively turned off when no longer needed (Lawrence et al., 2001; O'Dea and Hoffmann, 2010). Malfunction of the shutdown machinery might result in chronic inflammation, promoting pathologies such as inflammatory bowel disease (IBD) including ulcerative colitis (UC) and Crohn's disease (Majno and Joris, 2004; Kumar and Robbins, 2007). Although proper inflammatory response may suppress cancer (Mantovani et al., 2008), chronic inflammation can promote tumor initiation and progression (Brigati et al., 2002; Pikarsky et al., 2004; Grivennikov et al., 2010; Schetter et al., 2010; Ben-Neriah and Karin, 2011; Hanahan and Weinberg, 2011). Notably, IBD patients carry an increased cancer risk (Eaden et al., 2001).

NF-κB transcription factors consist of different dimeric combinations of p50, p52, p65 (RelA), c-Rel, and RelB, binding DNA as either hetero- or homodimers (DiDonato et al., 2012). Since only p65, c-Rel, and RelB contain transcriptional activation domains (TAD), dimers comprising these subunits can activate transcription while the others repress transcription unless they recruit specific co-activators (Heinz et al., 2013; Kogure et al., 2013). Additionally, NF-κB regulates diverse processes such as apoptosis, cell proliferation, differentiation, and tumorigenesis (DiDonato et al., 2012; Perkins, 2012).

Eukaryotic DNA is packaged in nucleosomes consisting of four core histones (H2A, H2B, H3, and H4), which undergo many post-translational modifications (PTM) that control chromatin dynamics and transcription (Campos and Reinberg, 2009). One such PTM is monoubiquitylation of mammalian histone H2B on lysine 120 (H2Bub1), executed primarily by the RNF20 (hBRE1)/RNF40 E3 ligase complex (Hwang et al., 2003).

H2Bub1 resides mainly downstream to transcription start sites (TSS), in preferential association with highly transcribed genes (Minsky et al., 2008). It participates in RNA polymerase II (RNA Pol II)-dependent transcription, cooperatively with the facilitates chromatin transcription (FACT) and polymerase-associated factor (PAF) complex (Pavri et al., 2006). H2Bub1 can also negatively regulate transcription and may contribute

to heterochromatin silencing (Zhang et al., 2008). In HeLa cells, H2Bub1 modulates transcription of specific gene sets (Shema et al., 2008): one subgroup, enriched in proto-oncogenes, is upregulated upon partial RNF20 depletion, while the other, including the p53 tumor suppressor, is downregulated. Furthermore, H2Bub1 impedes recruitment of TFIIS, a factor capable of relieving paused RNA Pol II (Shema et al., 2011). Conversely, H2Bub1 upregulates other transcripts by favoring recruitment of the SWI/SNF chromatin remodeling complex (Shema-Yaacoby et al., 2013).

Notably, RNF20 displays tumor suppressor features (Shema et al., 2008). Moreover, RNF20 and H2Bub1 are reduced in many cancers (Prenzel et al., 2011; Chernikova et al., 2012; Hahn et al., 2012; Urasaki et al., 2012; Thompson et al., 2013; Wang et al., 2013; Bedi et al., 2014). H2Bub1 levels are low in both embryonic and adult stem cells but increase during differentiation and may be a prerequisite for proper execution of the differentiation program (Fuchs et al., 2012; Karpiuk et al., 2012). Additionally, RNF20 and H2Bub1 are implicated in the DNA damage response, replication stress, and chromosomal stability (Kari et al., 2011; Moyal et al., 2011; Nakamura et al., 2011; Shiloh et al., 2011; Chernikova and Brown, 2012; Thompson et al., 2013).

H2Bub1 is coupled to ongoing transcription (Pavri et al., 2006; Zhang et al., 2008). Its modulation affects the transcriptional response to epidermal growth factor (EGF) (Shema et al., 2008), estrogen (Prenzel et al., 2011; Bedi et al., 2014), interferon gamma (Buro et al., 2010), and androgens (Jääskeläinen et al., 2012). We now report that RNF20 depletion, leading to decreased H2Bub1, augments the ability of the proinflammatory cytokine tumor necrosis factor alpha (TNF-α) to upregulate a panel of inflammation-associated genes. Importantly, mice with reduced RNF20 and H2Bub1 are predisposed to chronic colonic inflammation. Notably, colons of UC patients tend to underexpress *RNF20* and *RNF40* mRNA, in conjunction with H2Bub1 downregulation in both epithelial and stromal compartments. Moreover, RNF20-low mice succumb preferentially to inflammation-associated colorectal cancer (CRC) and their tumors exhibit reduced H2Bub1, as observed also in human CRC. Hence, attenuation of RNF20 and H2Bub1 may facilitate the emergence of chronic inflammation and subsequent cancer.

RESULTS

RNF20 Restricts NF-κB Target Gene Transcription in Response to TNF-α

To explore links between H2Bub1 and inflammation, we monitored H2Bub1 levels in cells exposed to TNF-α, employing non-transformed human mammary epithelial MCF10A cells. TNF-α downregulated transiently H2Bub1, both globally (Figures 1A and S1A) and at promoters and bodies of several cytokine genes (Figure S1B). This was not due to a decrease in *RNF20* mRNA (Figure S1C) or protein (Figure 1A). As expected, RNF20 knockdown caused substantial H2Bub1 loss (Figure S1A, siRNF20).

TNF-α transactivated many genes including *IL8* and *IL6*, as revealed by analysis of heterogeneous nuclear RNA (hnRNA) corresponding to primary transcripts (Figure 1B). Notably, RNF20 knockdown (Figure S1C) accelerated and prolonged this effect (Figure 1B), upregulating mature cytokine mRNA (Figures S1D and S1E). In contrast, RNF20 knockdown downregulated the non-inflammatory genes *p53* and *Bcl2* (Figure S1F). Hence RNF20, presumably through H2Bub1, restricts the activation of a set of inflammation-associated genes. Notably, knockdown of additional H2Bub1 machinery genes (RNF40 and hRAD6A) elicited similar effects (Figures S1G and S1H). Augmented cytokine gene expression was seen with three different RNF20 small interfering RNA (siRNA) oligos (Figure S1I), ruling out off-target effects.

In non-stimulated state, promoter regions of several proinflammatory cytokine genes are decorated with H3K9me3 (Figures 1C and S1J); this heterochromatin mark decreased transiently upon TNF-α exposure, concomitantly with the transcription wave (Figure S1J). Remarkably, H3K9me3 was selectively depleted from such promoters upon RNF20 knockdown, along with increased binding of paused (Ser5-phosphorylated) RNA Pol II (Figure 1D); this may underpin the accelerated transcriptional response to inflammatory stimuli (Figure 1B).

RNF20 Favors p50 Binding and Disfavors p65 Binding to κB Sites

Transcriptional induction of cytokine genes by TNF-α is largely mediated through NF-κB activation (Hayden and Ghosh, 2008; Ben-Neriah and Karin, 2011). Indeed, p65 depletion practically ablated the response (Figure S2A). The canonical NF-κB response to TNF-α employs primarily p65/p50 dimers (Hayden and Ghosh, 2012). Interestingly, rather than compromising *IL8* and *CXCL1* expression, p50 knockdown upregulated those genes (Figure S2B). Hence, in this system, repressive p50 homodimers may outweigh activating p65-containing dimers, while partial p50 depletion alleviates repression and promotes transcription by favoring p65-containing dimers. We therefore employed chromatin immunoprecipitation (ChIP)-qPCR to assess the association of p65 and p50 with relevant κB sites. In non-treated cells, p65 occupancy was very low, just above a control gene (*p21/CDKN1A)* lacking κB sites (Figure 2A). TNF-α increased p65 occupancy, which was further augmented by RNF20 depletion in *IL8* and *CXCL1*. RNF20 knockdown did not affect TNF-α-induced IκB degradation (Figure S2C) or p65 nuclear translocation (Figure S2D). However, it reduced basal and TNF-α-induced p50 binding, modestly in *IL6* and more strongly in *IL8* (Figure 2B), and affected differentially the global recruitment of NF-κB subunits to chromatin upon TNF-α treatment, favoring p65 over p50 (Figure 2C).

We next performed sequential ChIP ("re-ChIP"), reacting the chromatin first with anti-p65 and then anti-p50 antibodies. As expected, TNF-α increased the abundance of putative p65-p50 heterodimers (Figure 2D). Notably, this was further moderately augmented by RNF20 knockdown. Thus, RNF20 depletion alters the ratio between chromatin-associated NF-κB subunits in favor of p65, facilitating transcriptional activation.

RNF20 Downregulation Augments the TNF-α Response in Mouse Colonocytes, Intestinal Organoids, and Innate Immune Cells

To extend our observations to non-cancerous mouse epithelial cells, young adult mouse colonocytes (YAMC) (Whitehead

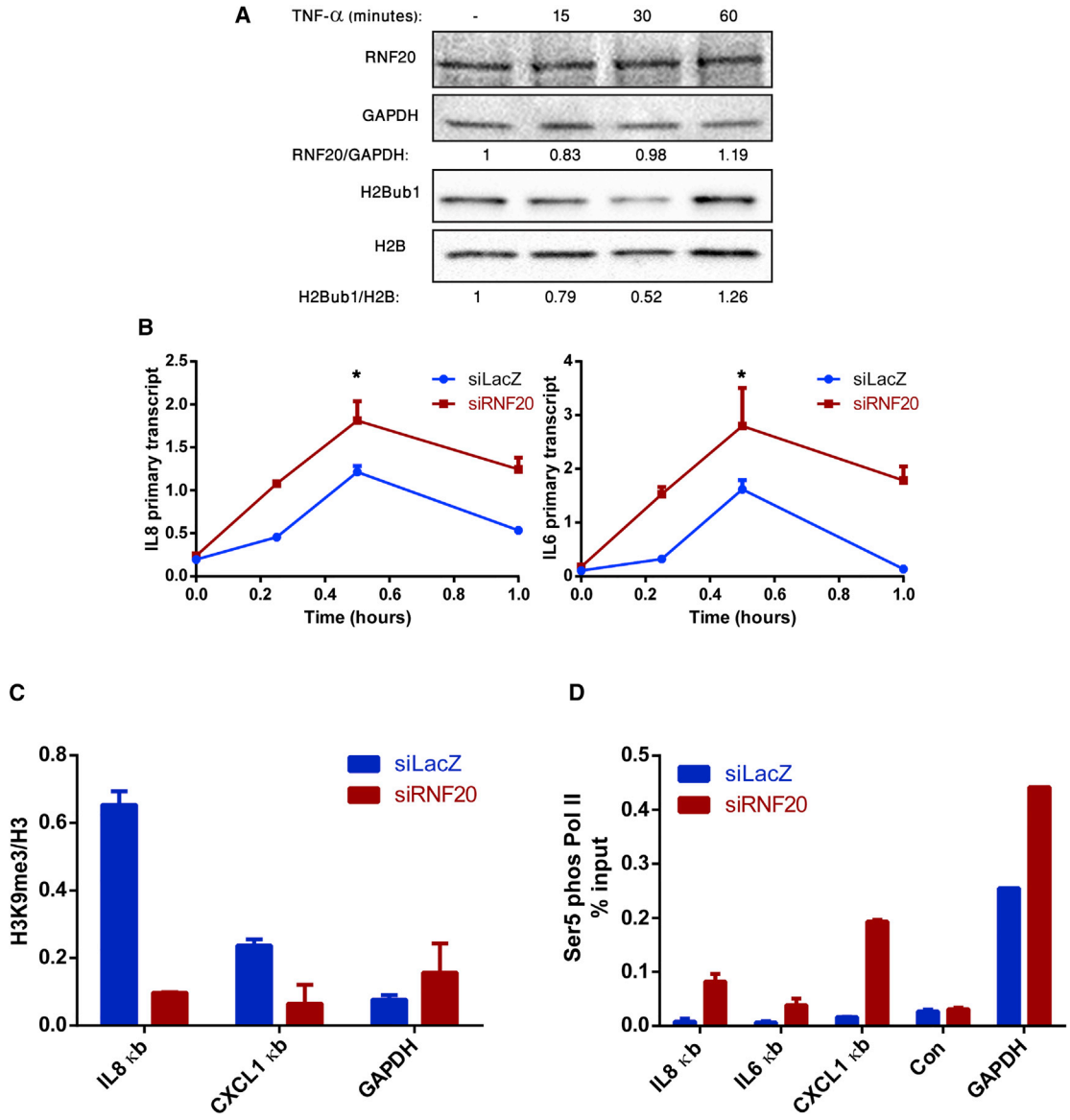

Figure 1. RNF20 Affects the Transcriptional Response of MCF10A Cells to TNF-α

(A) MCF10A cells were treated with 10 ng/ml TNF-α for different durations. RNF20, H2B, H2Bub1, and GAPDH were assessed by western blot analysis. Band intensities were quantified and the RNF20/GAPDH and H2Bub1/H2B ratios calculated. Similar results were obtained in six independent experiments.

(B) MCF10A cells were transfected with siRNA targeted against RNF20 or LacZ (control). 48 hours later, cells were treated with 10 ng/ml TNF-α for different durations. *IL8* and *IL6* hnRNA levels were determined by qRT-PCR, employing intron-derived primers. Values were normalized to *GAPDH* mRNA in the same sample. *$p < 0.05$. Error bars, SD. Similar results were obtained in four independent experiments.

(C) MCF10A cells transfected as in (B) were harvested and subjected to chromatin immunoprecipitation (ChIP) with H3 and H3K9me3 antibodies. Precipitated DNA was subjected to qRT-PCR analysis with primers spanning the κB site of the *IL8* and *CXCL1* genes, or *GAPDH*-derived primers as control. H3K9me3 values were normalized to H3 values. Error bars, SD. Similar results were obtained in three independent experiments.

(D) MCF10A cells transfected as in (B) were subjected to ChIP with antibodies specific for serine 5-phosphorylated RNA Pol II. Precipitated DNA was subjected to qRT-PCR analysis with primers spanning the κB site of the indicated cytokine genes, and primers derived from a non-transcribed genomic region (con) or *GAPDH* as controls. Values were normalized to input. Error bars, SD. Similar results were obtained in three independent experiments.

See also Figure S1.

et al., 1993) cells were employed. As in MCF10A cells, TNF-α elicited a rapid transient decrease in H2Bub1 also in YAMC cells (Figure 3A). As expected, RNF20 KD (Figure S3A) diminished H2Bub1 (Figure 3A). Notably, it augmented the induction of *IL6* and *KC* (a mouse homolog of *IL8*) (Figure 3B).

To investigate whether RNF20 affects inflammation in vivo, we attempted to generate RNF20 knockout mice utilizing embryonic stem cells carrying a gene trap insertion within the *RNF20* gene (see Supplemental Experimental Procedures); the insert is located between exons 17 and 18, and the predicted 97 kDa

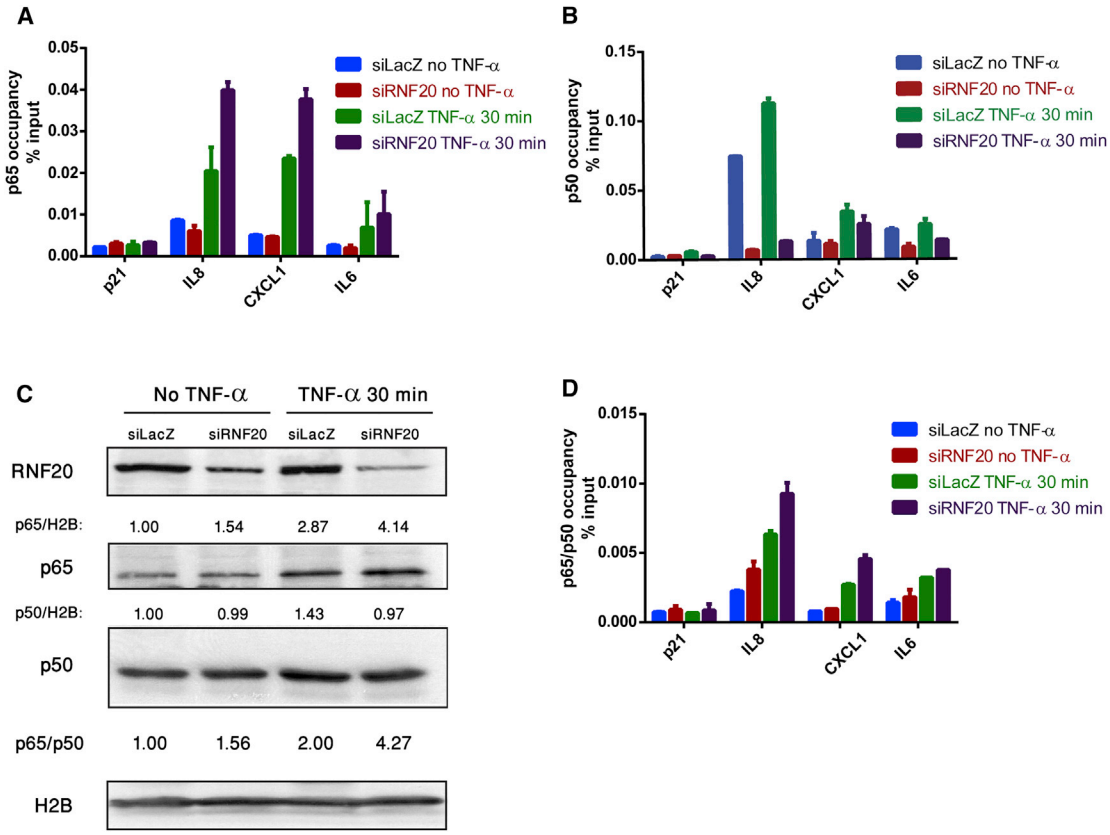

Figure 2. RNF20 Modulates NF-κB Chromatin Binding

(A) MCF10A cells were transfected with siRNA targeted against LacZ (control) or RNF20 for 48 hr and treated with 10 ng/ml TNF-α for 30 min. Cells were subjected to ChIP analysis with p65-specific antibodies. Precipitated DNA was subjected to qRT-PCR with primers spanning the κB sites of the *IL8*, *CXCL1*, and *IL6* genes or *CDKN1A* (*p21*)-derived primers as control. Values were normalized to input. Error bars, SD. Similar results were obtained in five independent experiments.

(B) MCF10A cells were transfected and analyzed as in (A), but employing p50-specific antibodies. Error bars, SD. Similar results were obtained in five independent experiments.

(C) MCF10A cells were transfected and treated with TNF-α as in (A). Total chromatin was enriched as described in Supplemental Experimental Procedures, and chromatin-associated RNF20, p50 and p65 was determined by western blot analysis. Numbers indicate relative intensities of the p50 and p65 bands after normalization to the corresponding H2B signal; ratios in the control (siLacZ) untreated sample were set as 1.0. Relative p65/p50 ratio was calculated accordingly. Similar results were obtained in three independent experiments.

(D) MCF10A cells were transfected and treated as in (A). Sequential chromatin immunoprecipitation (Re-ChIP) was performed as described in the Supplemental Experimental Procedures, employing p65 antibodies followed by p50 antibodies. qRT-PCR analysis was as in (A). Error bars, SD. Similar results were obtained in three independent experiments.

See also Figure S2.

protein should lack the C′ terminal RING domain. Such truncated protein was undetectable (Figure S3B), suggesting its intrinsic instability. Our attempts to obtain viable homozygous knockout progeny failed, owing to preimplantation embryonic lethality.

Heterozygous RNF20$^{+/-}$ mice were viable and appeared normal. We derived small intestinal 3D organoid cultures (Sato et al., 2011) from wild-type (WT) and RNF20$^{+/-}$ mice. As expected, RNF20$^{+/-}$ organoids had less *RNF20* mRNA and H2Bub1 than WT organoids (Figures 3C and S3C). Importantly, TNF-α elicited a rapid decrease in H2Bub1 (Figure 3C), and NF-κB target gene induction was augmented in RNF20$^{+/-}$ relative to WT organoids (Figures 3D and S3D). Likewise, peritoneal inflammatory leukocytes (mostly monocytes) and bone marrow-derived macrophages from RNF20$^{+/-}$ mice, underexpressing *RNF20* (Figures S3E and S3F), displayed an augmented TNF-α response at both RNA (Figures 3E and S3F) and secreted cytokine (Figure 3F) levels.

Thus, in non-cancerous epithelial cells, intestinal organoids, and innate immune cells, reduced RNF20/H2Bub1 augments the proinflammatory transcriptional response.

RNF20 Heterozygous Mice Are Prone to Severe Colonic Inflammation

Dextran sodium sulfate (DSS) is extensively used to study mouse colonic inflammation (Clapper et al., 2007). To explore the impact of RNF20 on inflammation in vivo, mice were exposed to 2% DSS (3 cycles, 5 days each; Figure 4A). Inflammation was assessed by colonoscopy, using a five-parameter scoring system (Becker et al., 2006) as described (Cooks et al., 2013). By day 7, inflammation became significantly more severe in

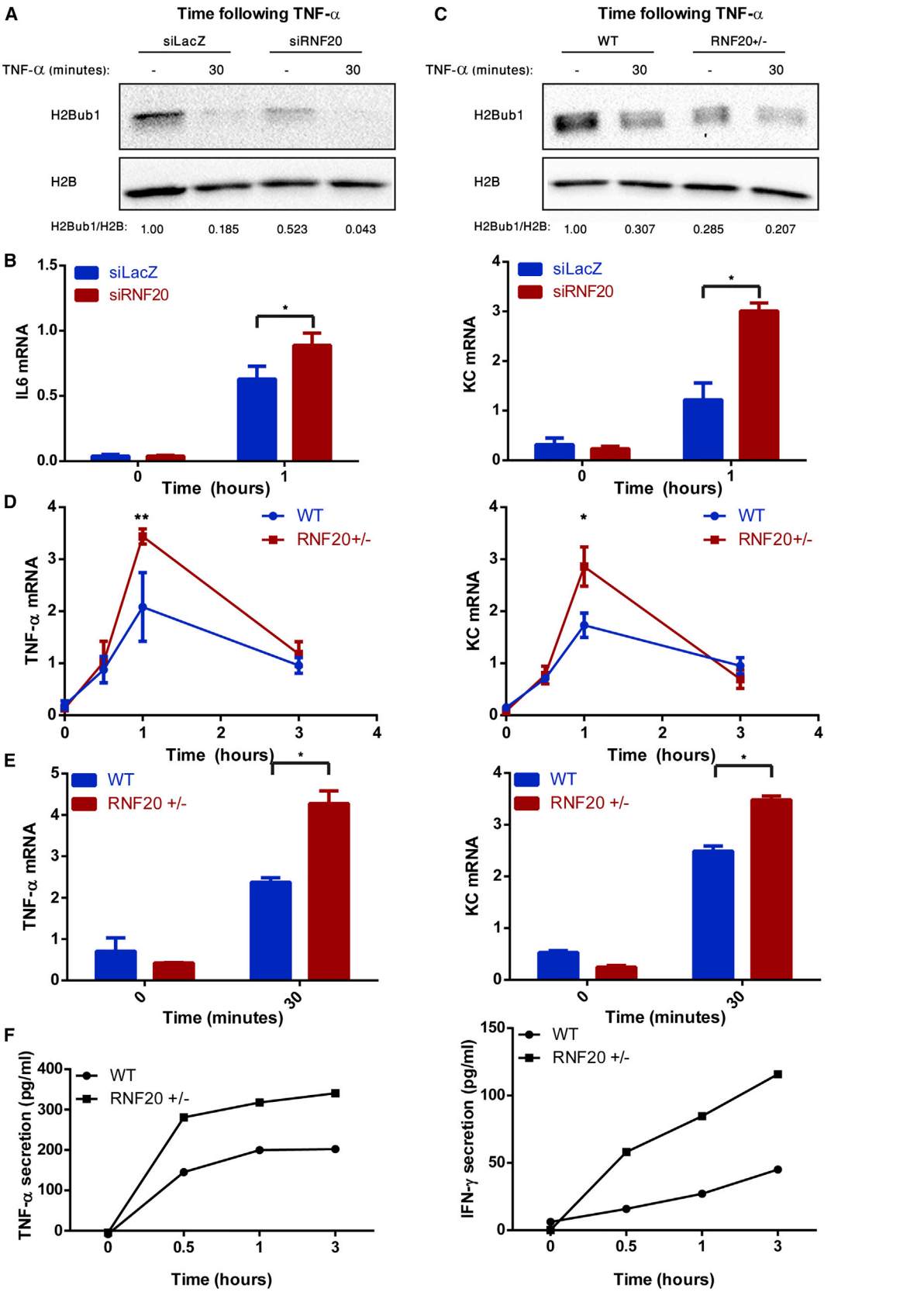

(legend on next page)

RNF20$^{+/-}$ colons than in WT colons (Figure 4B). Although inflammation subsided partially from day 65 onward, it remained higher in the heterozygotes. Moreover, by day 26 RNF20$^{+/-}$ mice displayed augmented splenomegaly (Figure 4C), and by day 65 they had shorter colons compared to WT mice (Figures 4D and S4A); both features persisted till day 180 (Figures S4B and S4C). Concordantly, DSS-treated RNF20$^{+/-}$ mice lost more weight than WT mice (Figure S4D). Thus, RNF20$^{+/-}$ mice are prone to augmented acute and chronic inflammation.

RNF20$^{+/-}$ mice express less RNF20 in all tissues. To assess the contribution of the bone marrow (BM)-derived compartment, we performed BM transplantation studies where BM of each genotype was transplanted into irradiated mice of each genotype. Reassuringly, WT mice reconstituted with WT BM were less inflamed than RNF20$^{+/-}$ mice reconstituted with RNF20$^{+/-}$ BM (Figure 4E). Interestingly, both WT mice reconstituted with RNF20$^{+/-}$ BM and RNF20$^{+/-}$ mice reconstituted with WT BM displayed intermediate inflammation, suggesting that both the intestinal epithelial compartment and the myeloid compartment contribute to the increased inflammation in RNF20$^{+/-}$ mice, consistent with the augmented cytokine responses in both cell types in vitro (Figures 3 and S3).

Remarkably, RNF20$^{+/-}$ colons had compromised barrier function, resulting in increased fluorescence in the blood of mice force-fed dextran FITC (Figure 4F). This intestinal leakiness, perhaps due to reduced expression of tight junction genes (e.g., cingulin, Figure S4E), may offer an additional explanation for the epithelial contribution to the augmented inflammation. Interestingly, c-Myc expression was elevated in RNF20$^{+/-}$ colons (Figure S4E).

Although average *RNF20* mRNA levels in RNF20$^{+/-}$ colons and lungs (Figures S4F and S4G) was approximately half that of WT mice, it varied greatly among individual mice (Figure 4G). H2Bub1 correlated well with *RNF20* mRNA (Figure S4H). Remarkably, regardless of genotype, *RNF20* mRNA levels (measured in the non-inflamed lungs) were strongly inversely correlated with colonic inflammatory score (Figure 4G), as seen also with interferon gamma (IFN-γ) secretion from colon slices at day 7, *MIP2* mRNA expression at day 26, and colon length and spleen weight at day 180 (Figures S4I–S4L). This argues strongly that the increased inflammation in RNF20$^{+/-}$ mice is indeed due to the actual downregulation of RNF20 (and presumably H2Bub1).

Increased MDSC Activation in RNF20$^{+/-}$ Mice

Under inflammatory conditions, immune cells infiltrate the colonic epithelium. Notably, immune patches composed mainly of T cells, B cells, and macrophages were more abundant in DSS-treated RNF20$^{+/-}$ than in WT mice (Figures S5A and S5B). RNF20$^{+/-}$ mice displayed more infiltrating macrophages (F4/80 positive, Figures S5C and S5D), including M2 macrophages (CD206^{+}, Figure 4H), as well as more T cells (CD3^{+}, Figures S5E and S5F), at both day 26 and 65. Importantly, RNF20-deficient mice had more myeloid-derived suppressor cells (MDSCs), identified by IHC staining for CD11b^{+} and Gr1 (Figure 4I) and CD11b positivity by FACS (Figure S5G). Those MDSCs were more active, producing excessive ROS and nitric oxide (Figure S5H) and overexpressing *Arginase 1* (Figure S5I). Furthermore, T cell receptor ζ chain was downregulated in RNF20$^{+/-}$ splenic T cells (Figure S5J), indicative of impaired T cell function. CD3 epsilon was comparable in WT and RNF20$^{+/-}$ mice (Figure S5J), further arguing that the reduced T cell functionality in the latter is mediated by MDSCs. Importantly, RNF20$^{+/-}$ MDSCs revealed a significantly greater capacity to downregulate ζ chain levels in co-incubated naive T cells (Figure 4J). Hence, reduced RNF20/H2Bub1 might promote immunosuppression via increased MDSC activation.

Elevated NF-κB Activity and DNA Damage in RNF20$^{+/-}$ Mice

Consistent with the enhanced NF-κB activation in cultured cells, inflamed colons of RNF20$^{+/-}$ mice revealed stronger nuclear p65 staining than WT mice, while p50 exhibited an opposite trend (Figure 5A). Nuclear γ-H2AX foci, indicative of DNA damage, were more abundant in RNF20$^{+/-}$ colons (Figure 5B), probably reflecting the combined effect of increased DNA-damaging ROS (Schetter et al., 2010) and compromised DNA double strand break repair (Chernikova et al., 2010; Moyal et al., 2011; Nakamura et al., 2011). Notably, despite the marked increase in apparent DNA damage, p53 was only mildly elevated (Figure 5B); p21, the canonical p53 target gene, was hardly induced at all. This suggests a compromised p53 response, probably due to p53 mRNA downregulation in RNF20$^{+/-}$ mice (Figure S4E). Thus, while RNF20$^{+/-}$ colonocytes accumulate more DNA damage, their ability to mount a full DNA damage response is compromised, potentially exacerbating genomic instability.

Figure 3. Reduced RNF20 Augments the TNF-α Response in Mouse Cells, Intestinal Organoids, and Peritoneal Inflammatory Leukocytes

(A) YAMC (young adult mouse colonocytes) cells were transfected with siRNA targeted against *RNF20* or *LacZ* as control and either treated or not treated with 10 ng/ml TNF-α for 30 min. H2B and H2Bub1 levels were assessed by Western blot analysis. Similar results were obtained in five independent experiments.

(B) YAMC cells were transfected as in (A). Forty-eight hours later, cells were treated with 10 ng/ml TNF-α for 1 hr. *IL6* and *KC* mRNA levels were determined by qRT-PCR, and normalized to β-*actin* mRNA in the same sample. *$p < 0.05$. Error bars, SD. Similar results were obtained in five independent experiments.

(C) Small intestine organoids from WT or RNF20$^{+/-}$ mice were either treated or not treated with 10 ng/ml TNF-α for 30 min. H2B and H2Bub1 levels were assessed by western blot analysis. The H2B and H2Bub1 panels are from two separate gels loaded with identical aliquots of the same extract. Similar results were obtained in four independent experiments.

(D) Small intestine organoids from WT or RNF20$^{+/-}$ mice were treated with 10 ng/ml TNF-α for different durations. Cytokine mRNA levels were determined by qRT-PCR and normalized to β-*actin* mRNA in the same sample. *$p < 0.05$, **$p < 0.01$. Error bars, SE. The graph represents average of four independent experiments.

(E) Mice were injected intraperitoneally with 4% thioglycolate. Four days later, peritoneal inflammatory leukocytes were collected and either treated or not treated with 10 ng/ml TNF-α for 30 min. Cytokine mRNA levels were determined by qRT-PCR and normalized to β-*actin* mRNA in the same sample. *$p < 0.05$. Error bars, SD. Similar results were obtained in three independent experiments.

(F) Mice were injected intraperitoneally with 4% thioglycolate. Four days later, peritoneal inflammatory leukocytes were removed and treated with 10 ng/ml TNF-α for different durations. Secreted cytokines were quantified by ELISA. Similar results were obtained in three independent experiments.

See also Figure S3.

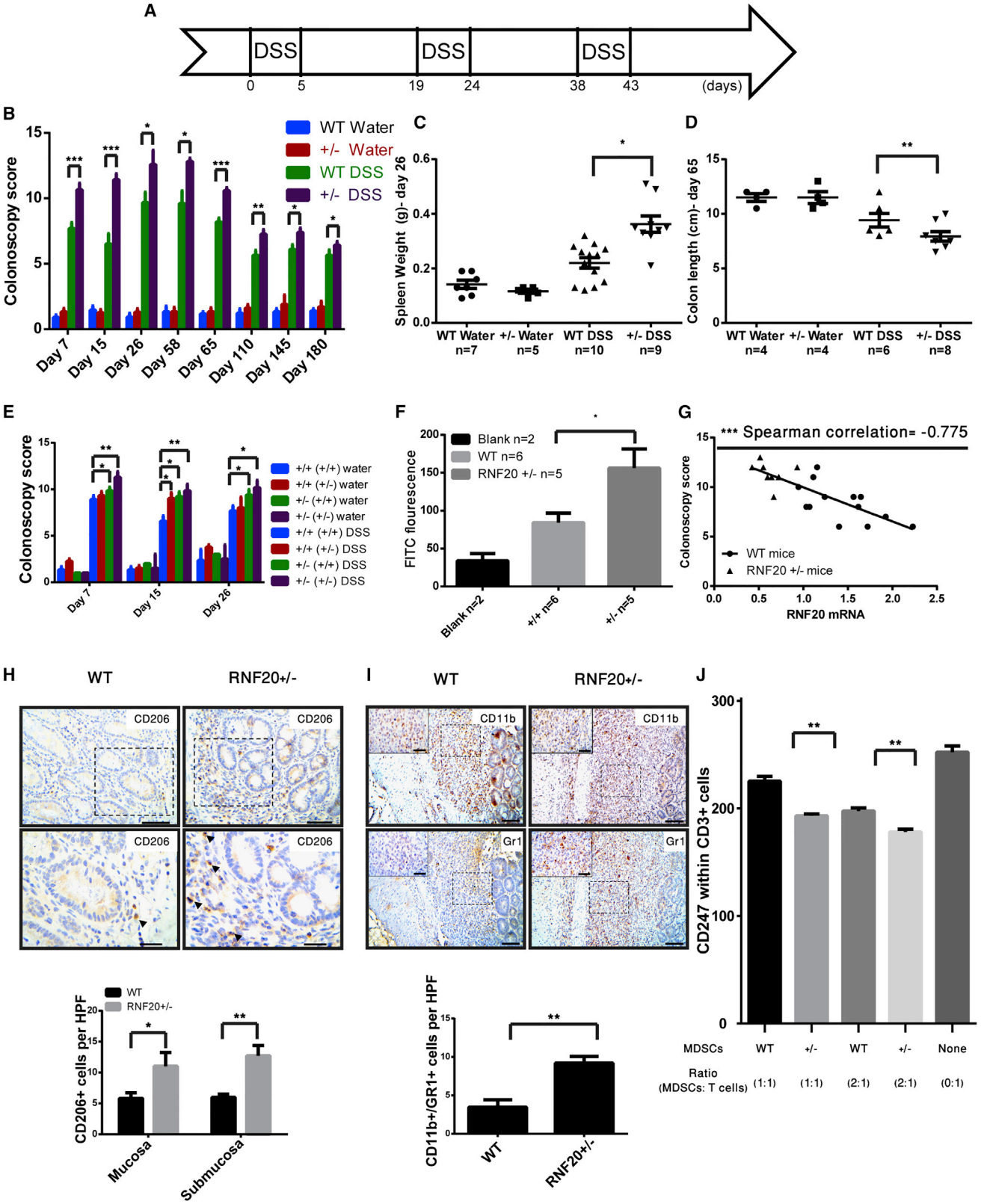

(legend on next page)

RNF20$^{+/-}$ Mice Are Predisposed to Inflammation-Associated Colorectal Tumors

Chronic colonic inflammation promotes colorectal cancer (Terzić et al., 2010; Ullman and Itzkowitz, 2011). In the mouse, this is greatly enhanced by combining DSS with the chemical carcinogen azoxymethane (AOM) (Ward et al., 1973; Tanaka et al., 2003). We therefore injected mice with AOM (1 μg/g body weight) 7 days prior to DSS exposure (Figure 6A). Colonoscopy revealed more polyps in RNF20$^{+/-}$ mice than in WT mice (Figure 6B; representative images in Figure S6A). Moreover, while RNF20$^{+/-}$ adenomas often progressed to carcinoma by day 180, none did in WT mice (Figure 6C, DSS-AOM). Likewise, DSS alone elicited carcinomas by day 180 in several RNF20$^{+/-}$ but no WT animals (Figure 6C, DSS). Some RNF20$^{+/-}$ mice developed mucinous carcinoma with neoplastic glands invading the submucosa and penetrating the muscularis propria (T2), indicative of an aggressive course (Figure S6B). Hence, reduced RNF20 promotes both initiation and progression of inflammation-associated CRC in mice. Notably, the impact of partial RNF20 depletion on tumor progression was more pronounced than on inflammation. Thus, beyond augmented inflammation, additional effects of RNF20 shortage might also promote cancer in this setting.

While total H2B staining was similar in tumors and non-tumorous crypts (Figure 6D, left panels), polyps and carcinomas in both genotypes often displayed reduced H2Bub1 in both epithelial and stromal compartments (Figures 6D, 6E, and S6C, arrows), implying that colorectal tumorigenesis is associated with further H2Bub1 decrease.

Lower H2Bub1 May Promote Human Ulcerative Colitis and Colorectal Cancer

To evaluate the human relevance of our findings, we analyzed a gene expression array including data from 27 healthy people, 35 UC patients with non-inflamed colons, and 38 UC patients with inflamed colons (Sen and Bhaumik, 2013). For patients sampled multiple times, mean values were used. Remarkably, UC colons had reduced *RNF20* and *RNF40* mRNA (Figure 7A). Moreover, *RNF20* and *RNF40* were inversely correlated with several inflammatory cytokine mRNAs, including *IL6* and *IL8* (Figures S7A and S7B; Table S1), consistent with the notion that H2Bub1 downregulation drives chronic inflammation and NF-κB activation also in humans. In agreement, H2Bub1 was markedly reduced in IBD patient colonic epithelium, and to a lesser degree, also in the stromal compartment, relative to non-specific mild chronic colitis (NSC) (Figures 7B and 7C). This raises the intriguing possibility that constitutively reduced RNF20/RNF40, leading to partial H2Bub1 depletion, may predispose humans to particular chronic inflammatory diseases.

Mouse colonic tumors exhibited reduced H2Bub1 (Figure 6D). Consistent with earlier observations (Urasaki et al., 2012), a similar pattern was revealed in human CRC tissue microarrays (Figures 7D and 7E) and colitis-associated cancer (CAC) samples (Figure S7C). Specifically, H2Bub1 in the cancer cells declined along disease progression (Figures 7F and S7D). Interestingly, partial H2Bub1 downregulation was often seen also in the tumor stroma, although no further reduction occurred as cancer progressed (Figures 7D and 7F). Significantly, analysis of TCGA (http://www.cbioportal.org/public-portal/) colon adenocarcinoma gene expression data, comparing normal and tumor samples from the same patients, revealed lower *RNF20* and *RNF40* mRNA in the cancer tissue (Figure 7G). Thus, H2Bub1 is often reduced in human CRC, partly owing to compromised *RNF20/40* expression, corroborating the human relevance of our mouse model.

DISCUSSION

In cultured cells, TNF-α elicits a rapid transient decrease in global H2Bub1, preceding the induction of NF-κB target genes. RNF20 depletion enhances NF-κB-dependent transcription of specific cytokine genes, suggesting that TNF-α-induced H2Bub1 downregulation facilitates the ensuing NF-κB response.

Figure 4. RNF20$^{+/-}$ Mice Are More Prone to Acute and Chronic Colonic Inflammation

(A) Timeline of the chronic DSS protocol.

(B) Eight-week-old male WT or RNF20$^{+/-}$ mice weighing 22–28 g were treated with 2% DSS as outlined in (A). To monitor inflammation, mice were anesthetized with 10% xylene and 10% ketamine, and colonoscopies were performed as indicated. Inflammation scores were calculated as described in Experimental Procedures.*$p < 0.05$, **$p < 0.01$, ***$p < 0.001$. Error bars, SE. At least eight mice of each group were analyzed.

(C) Spleens of either WT or RNF20$^{+/-}$ mice were collected at day 26 and weighed. *$p < 0.05$. n, number of mice per group. Error bars, SE.

(D) WT and RNF20$^{+/-}$ mice were sacrificed at day 65 and colon lengths were measured. **$p < 0.01$. n, number of mice per group. Error bars, SE.

(E) Six-week-old male mice were sub-lethally irradiated to deplete bone marrow (BM) cells, and injected with BM cells derived from either WT or RNF20$^{+/-}$ mice. Mice were then treated with DSS as outlined in (A). Inflammation was monitored as in (B). *$p < 0.05$, **$p < 0.01$. Error bars, SE. At least six mice of each group were analyzed. The genotypes of the irradiated recipient mice and the donor BM are indicated without brackets and in brackets, respectively.

(F) Non-treated WT and RNF20$^{+/-}$ mice were force fed dextran-FITC by gavage. Fluorescence intensity in the blood was measured 6 hr later. Blank, background fluorescence in mice not injected with dextran-FITC. *$p < 0.05$. Error bars, SE.

(G) RNA was extracted from lungs of WT and RNF20$^{+/-}$ mice as described in the Supplemental Experimental Procedures. *RNF20* mRNA levels in lungs of individual mice were plotted against the corresponding colonoscopy scores. Spearman correlation coefficient = −0.775, ***$p < 0.001$.

(H) Colons of DSS-treated RNF20$^{+/-}$ and WT mice collected at day 26 were subjected to IHC staining for CD206. Lower panels show a higher magnification of the dashed area in upper panels. Arrowheads indicate positive nuclei. Lower magnification scale bars, 100 μm; higher magnification scale bars, 50 μm; bottom, quantification based on six WT mice and five RNF20$^{+/-}$ mice; HPF, high power field. *$p < 0.05$, **$p < 0.01$. Error bars, SE.

(I) Colons of DSS-treated WT and RNF20$^{+/-}$ mice collected at day 26 were subjected to IHC staining for CD11b and Gr1. Insets: a higher magnification of the dashed area. Lower magnification scale bar, 100 μm; higher magnification scale bar, 50 μm; bottom, quantification based on six WT mice and five RNF20$^{+/-}$ mice; HPF, high power field. **$p < 0.01$. Error bars, SE.

(J) Spleens of DSS-treated WT and RNF20$^{+/-}$ mice were collected at day 26. MDSCs were isolated and incubated with naive T cells from spleens of untreated RNF20$^{+/-}$ mice as described in the Supplemental Experimental Procedures, at the indicated MDSC:T cell ratio. Cells were then subjected to FACS-based analysis of CD247 (T cell receptor zeta chain) within CD3^{+} cells. **$p < 0.01$. Error bars, SE.

See also Figures S4 and S5.

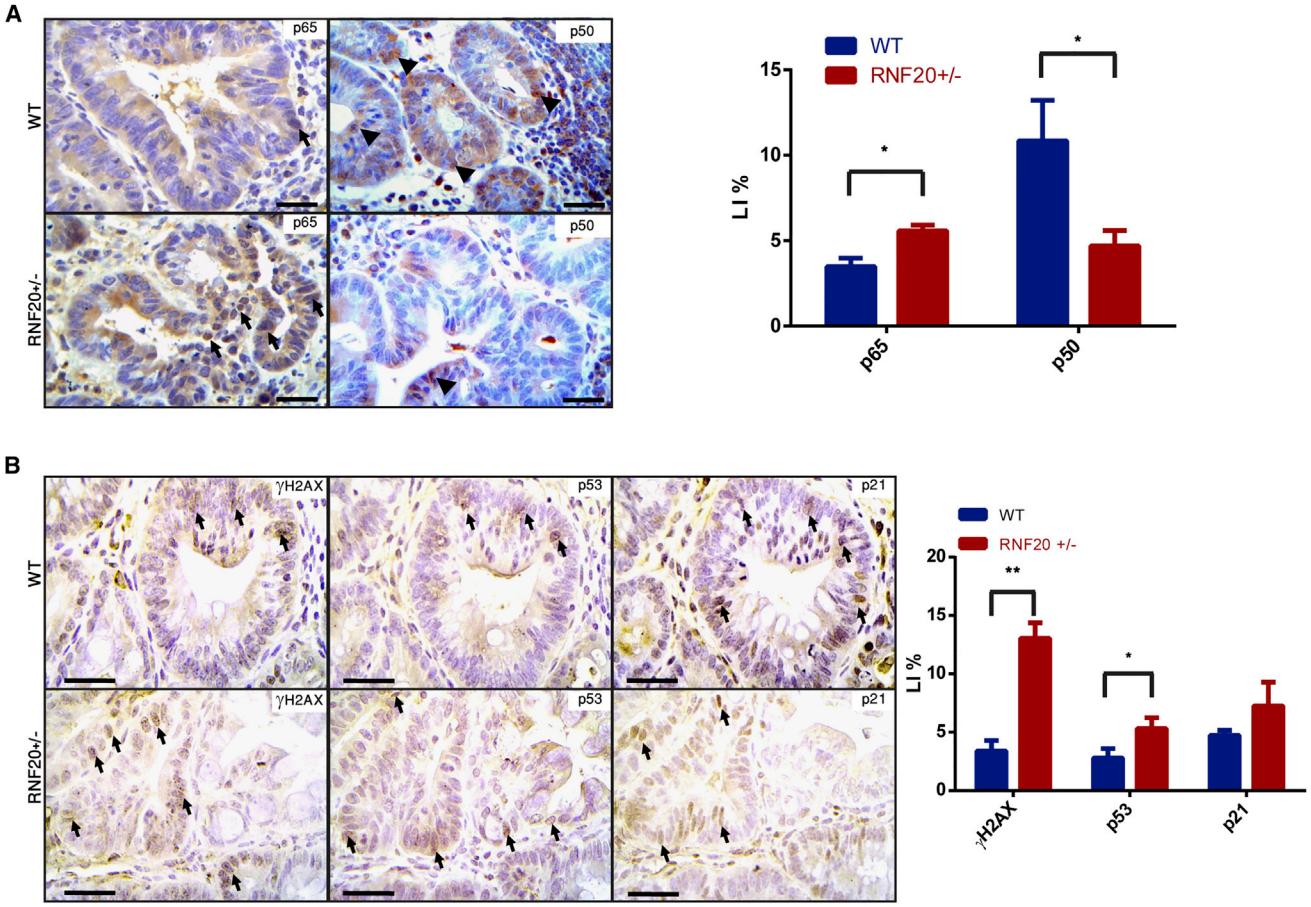

Figure 5. Increased NF-κB Activation and DNA Damage in RNF20$^{+/-}$ Mice

(A) Colons sections of DSS-treated WT and RNF20$^{+/-}$ mice collected at day 26 were stained for p65 and p50. Arrowheads denote positive nuclei. Scale bar, 50 μm. LI%, labeling index. *$p < 0.05$. Error bars, SE. Right panel: quantification based on five WT and six RNF20$^{+/-}$ mice.

(B) Colons of DSS-treated WT and RNF20$^{+/-}$ mice collected at day 26 were subjected to IHC staining for γ-H2AX, p53 and p21. Arrowheads denote positive nuclei. Scale bar, 50 μm. LI%, labeling index. *$p < 0.05$, **$p < 0.01$. Error bars, SE. Right panel: quantification based on three WT and four RNF20$^{+/-}$ mice.

The subsequent recovery of H2Bub1 might serve to tune down the NF-kB response. Consequently, constitutively reduced H2Bub1 might hamper efficient shutoff, resulting in prolonged "leaky" NF-kB activation. Notably, although H2Bub1 is the most likely mediator of the effects of RNF20, a contribution of additional RNF20 substrates cannot be ruled out presently.

The abundance of H2Bub1 on chromatin can dictate selective binding of numerous transcription-associated factors (Shema-Yaacoby et al., 2013). By altering chromatin architecture (Fierz et al., 2011), H2Bub1 may favor binding of p50 homodimers over p50-p65 heterodimers or p65 homodimers. Notably, downregulation of RNF20 and H2Bub1 reduces the heterochromatin mark H3K9me3 in the promoter region of affected cytokine genes (Figure 1C) and enables efficient Pol II recruitment (Figure 1D). This might involve the histone H3K9 methyltransferase EHMT1, which interacts constitutively with p50 homodimers (Ea et al., 2012). TNF-α-induced downregulation of H2Bub1 might also facilitate the binding of the transcription elongation factor TFIIS (Shema et al., 2011). Lacking a functional TAD, p50 homodimers might repress NF-κB activity (Heinz et al., 2013; Kogure et al., 2013), keeping cytokine genes off in the absence of activation signals. When encountering an activation signal, H2Bub1 levels rapidly decrease; we propose that this attenuates the association of p50 homodimers with chromatin, favoring recruitment of transactivation-competent p65-containing dimers. Interestingly, human tumors often underexpress p50, probably fostering cancer progression (Kravtsova-Ivantsiv et al., 2015).

The modular role of H2Bub1 is not limited to TNF-α. Indeed, H2Bub1 and RNF20 also affect the transcriptional response to EGF and IFN-γ (Shema et al., 2008; Buro et al., 2010). H2Bub1 is more dynamic than other histone modifications (Fuchs et al., 2014); hence, rapid alterations in H2Bub1 may guide changes in other histone modifications (Zhu et al., 2005; Nakachi et al., 2013).

RNF20$^{+/-}$ mice display increased susceptibility to colonic inflammation and inflammation-associated cancer. Since RNF20$^{+/-}$ mice are heterozygous in all tissues, the elevated inflammation may be due to H2Bub1-dependent changes not only in the gut epithelium but also in other host components

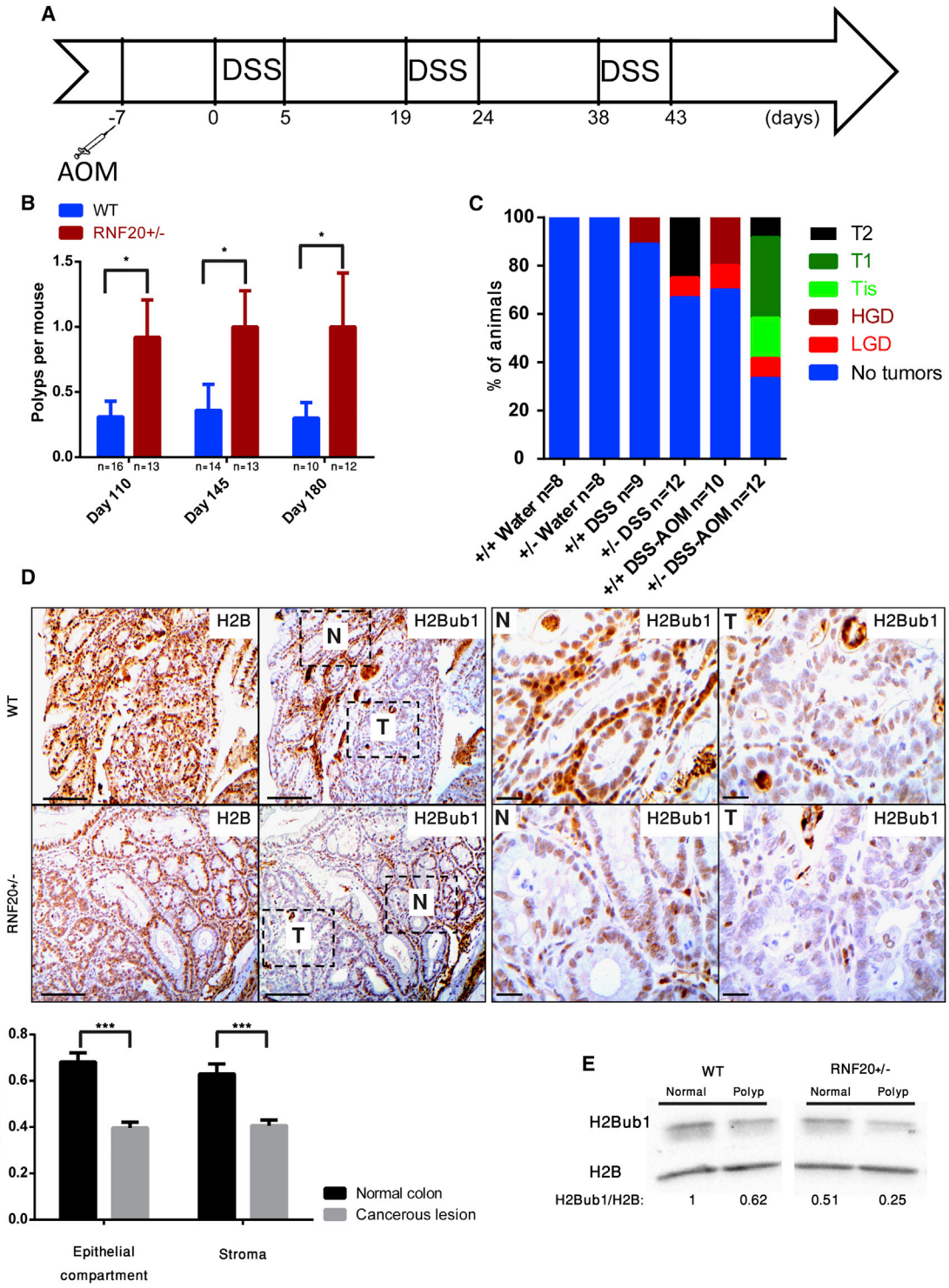

Figure 6. RNF20$^{+/-}$ Mice Are Predisposed to Colonic Tumorigenesis

(A) Timeline of the DSS-AOM protocol.

(B) Eight-week-old male mice weighing 22–28 g were treated with 1 μg/g AOM plus 2% DSS as described in (A). Polyps were monitored by colonoscopy on the indicated days. *$p < 0.05$. Error bars, SE.

(C) Colons of WT and RNF20$^{+/-}$ mice, treated as indicated at the bottom, were collected at day 180 and subjected to histopathological analysis. Bars depict the percentage of mice with the indicated lesions within a given treatment group; in mice with more than one type of lesion, only the most advanced lesion was

(legend continued on next page)

such as immune cells, a notion supported by the enhanced TNF-α response of RNF20$^{+/-}$ inflammatory leukocytes and macrophages (Figures 3E, 3F, and S3F), as well as by the bone marrow chimera experiments. Furthermore, we cannot exclude RNF20/H2Bub1 effects on gut microflora.

Notably, *RNF20* mRNA levels varied greatly between individual mice (Figure 4G), and inflammation inversely correlated with *RNF20* mRNA irrespective of genotype. This raises the intriguing possibility that in humans, where inter-individual differences in H2Bub1 levels are likely broader than in inbred mice, such inherent differences might affect susceptibility to chronic inflammatory diseases. Indeed, human ulcerative colitis (UC) is significantly associated with reduced *RNF20/40* expression (Figure 7A), and lower *RNF20/40* correlates with augmented inflammatory cytokine expression in human CRC (Figures S7A and S7B; Table S1).

Remarkably, both with DSS alone and with DSS+AOM, aggressive tumors were observed exclusively in RNF20$^{+/-}$ but not WT mice (Figure 6C). Indeed, as in our mouse tumors, many human sporadic CRC tumors exhibit reduced H2Bub1 (Urasaki et al., 2012), which declines as tumors progress (Figures 7D–7F). Reduced *RNF20* and *RNF40* mRNA in human CRC (Figure 7G) provides at least one plausible mechanistic explanation for the frequent depletion of H2Bub1. Conceivably, compromised H2Bub1 probably contributes to colorectal carcinogenesis by more than just augmenting inflammation. H2Bub1 facilitates DNA repair (Moyal et al., 2011; Nakamura et al., 2011; Shiloh et al., 2011); indeed, RNF20$^{+/-}$ mice display elevated γ-H2AX (Figure 5B), suggesting exacerbated DNA damage. Furthermore, RNF20$^{+/-}$ mice exhibit abundant M2 macrophages, providing a tumor supportive environment. Importantly, they display enhanced recruitment and augmented activation of MDSCs, which suppress anti-tumoral T cell activity and thereby facilitate tumor progression (Katoh et al., 2013). Such non-cell autonomous effects of reduced RNF20 might underpin the increased tumor progression in RNF20$^{+/-}$ mice as well as the association between lower H2Bub1 and advanced human cancer.

Stem cells (SCs) typically display low H2Bub1, which increases markedly during SC differentiation and is required for their differentiation (Fuchs et al., 2012; Karpiuk et al., 2012). Hence, reduced H2Bub1 might also increase the tendency of colonic epithelial cells to adopt stem cell-like features. Of note, NF-κB has a crucial role in crypt stem cell expansion (Myant et al., 2013; Schwitalla et al., 2013). Intriguingly, like RNF20, the stem cell E3 ligase RNF43 has also been implicated in colonic tumor suppression (Koo et al., 2012).

In sum, our study highlights non cell-autonomous functions of H2Bub1 and implies that low H2Bub1 favors inflammation and cancer. It remains to be determined whether, like in mice, also in humans inter-individual variations in constitutive H2Bub1 levels may be a risk factor for UC and CRC and perhaps additional inflammatory diseases and inflammation-associated cancers.

EXPERIMENTAL PROCEDURES

Cell Culture and siRNA Transfections

MCF10A cells were cultured at 37°C in DMEMF-12 medium (Biological Industries) supplemented with penicillin and streptomycin as well as 10 μg/ml insulin, 0.1 μg/ml cholera toxin, 0.5 μg/ml hydrocortisone, 5% heat-inactivated horse serum, and 10 ng/ml EGF. YAMC cells were cultured at 32°C in RPMI-1640 (Biological Industries) supplemented with penicillin and streptomycin and 10^{-6} M hydrocortisone, 10^{-5} M α-thioglycerol, 1 μg/ml insulin, 5 units/ml mouse INF-γ, and 5% fetal calf serum. Small intestine organoids were prepared as described (Sato et al., 2011).

siRNA-mediated knockdown was with Dharmafect 1 reagent according to the manufacturer's protocol (Dharmacon RNAi technologies, Thermo Fisher Scientific). siRNA oligonucleotide SmartPools (siLacZ, siRNF20, si-p65, si-p50, siRNF40, and siRad6) were from Dharmacon. Final concentration of all siRNA oligonucleotides was 25 nM. TNF-α from R&D Systems was applied at a final concentration of 10 ng/ml. Cells were washed twice with cold PBS, harvested, centrifuged for 2 min at 4,000 RPM, and frozen at −80°C until lysis.

Mouse Handling

DSS treatment, colonoscopy, and analysis of mouse tissues were as described (Cooks et al., 2013). Azoxymethane (Wako Chemicals, 011-20171; 1 μg/g) was injected intraperitoneally (i.p.) 7 days prior to the first DSS treatment. For bone marrow (BM) transplantation, mice were irradiated with 950 rad and injected intravenously with 5×10^6 BM-derived cells. Mice were then treated for 6 weeks with Ciproxin and subjected to DSS treatment. For intestinal permeability experiments mice were force fed by gavage with Dextran FITC (T7816, Sigma-Aldrich; 0.6 g/g). After 6 hr, mice were bled and blood fluorescence intensity was measured. Procedures involving animals conformed to institutional guidelines approved by the Animal Ethics Committee of the Weizmann Institute (IACUC 00800211-1).

Inflammation severity and polyps were scored by colonoscopy according to a previously published five- parameter scoring system (Becker et al., 2006); data was analyzed with the R statistical analysis software, employing ANOVA. H&E slides of each mouse were analyzed by two independent pathologists, and tumors were scored according to their grade: low grade dysplasia (LGD), high grade dysplasia (HGD), carcinoma in situ (Tis), tumor invading the submucosa (T1), and tumor invading the muscularis propria (T2).

To obtain peritoneal inflammatory leukocytes, mice were injected i.p. with 4% thioglycolate. Four days later, leukocytes were collected from mouse peritoneum and plated in a tissue culture dish.

Human Ethical Issues

Primary colon biopsies for IHC studies were obtained from Hebrew University-Hadassah Medical Center under approval by the Institutional Review Board (HMO-0145-13), verifying that informed consent is not required.

SUPPLEMENTAL INFORMATION

Supplemental Information includes Supplemental Experimental Procedures, seven figures, and one table and can be found with this article online at http://dx.doi.org/10.1016/j.celrep.2016.01.020.

considered. LGD, low grade dysplasia; HGD, high grade dysplasia; Tis, carcinoma in situ; T1, carcinoma invading the submucosa; T2, carcinoma invading the muscularis propria; n, number of mice per group.

(D) Colons of DSS+AOM-treated mice of the indicated genotype were collected at day 65. Consecutive slides were stained for H2B and H2Bub1, respectively. N, normal tissue; T, tumor. Panels on the right show a higher magnification of the dashed areas in the left H2Bub1 panels. Scale bars, 200 μm for lower magnification, 25 μm for higher magnification. Lower panel: quantification based on eight WT and ten RNF20$^{+/-}$ mice. ***$p < 0.001$. Error bars, SE.

(E) Colons of DSS+AOM-treated mice of the indicated genotypes were collected at day 180. Polyps and adjacent normal tissue were extracted and subjected to western blot analysis for H2Bub1 and H2B.

See also Figure S6.

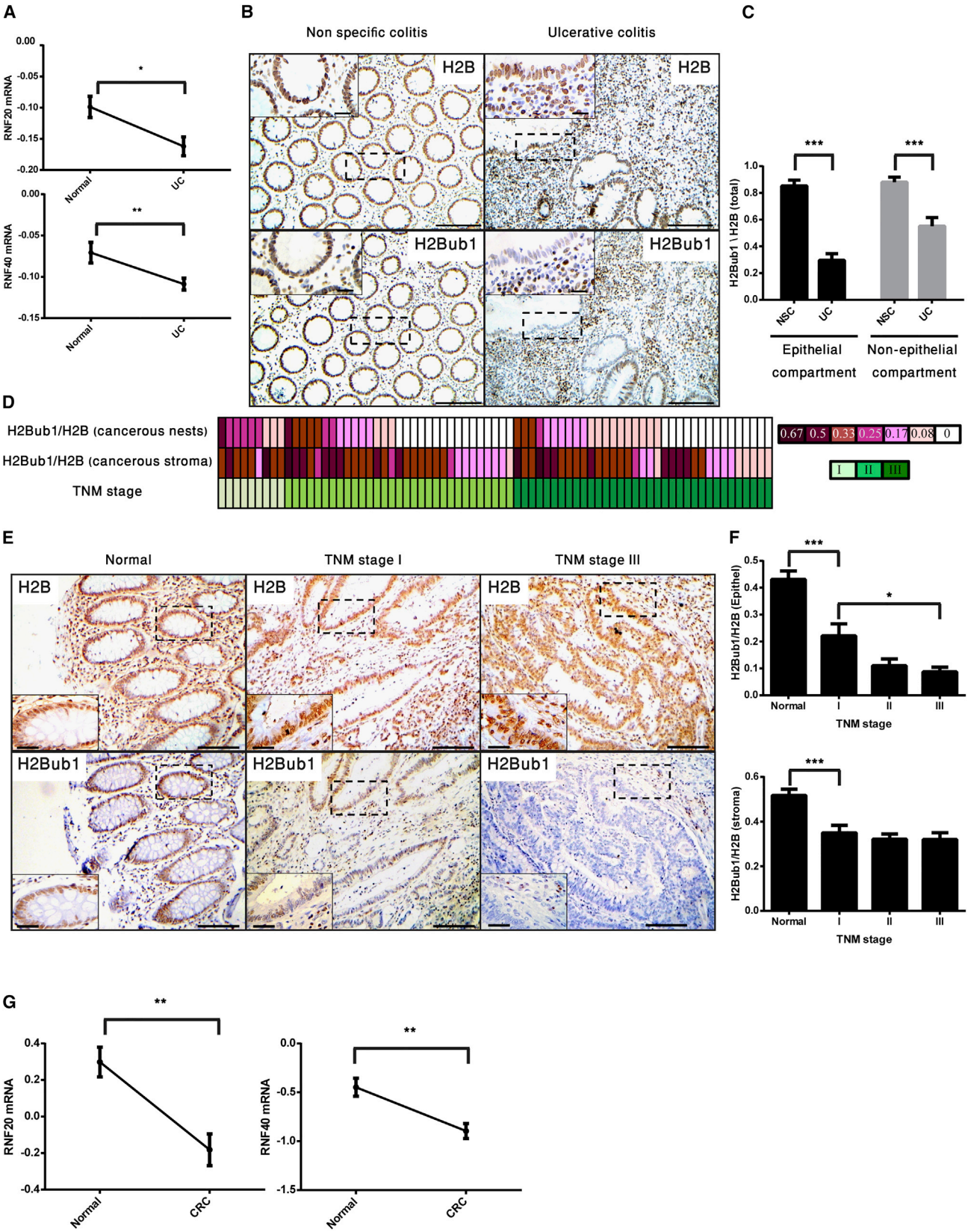

(legend on next page)

AUTHOR CONTRIBUTIONS

O.T. designed and performed the experiments, and wrote the manuscript. T.C. provided advice and helped in conducting experiments. E.S. generated the RNF20 knockout mice. I.P. and V.G. conducted histological staining and analysis. E.P. and A.H. conducted pathological analysis and provided suggestions for further analyses. M.B., J.K., H.A., and H.B. conducted the experiments presented in Figures 4J, S5G, S5H, and S5J. R.R. conducted bio-statistical analysis of human data. M.O. supervised the work and wrote the manuscript.

ACKNOWLEDGMENTS

We thank Steven A. Johnsen for the kind gift of antibodies, Neil Perkins, Fiona Oakley, Intidhar Galy, and Ronny Drapkin for helpful suggestions and reagents, and Hagai Marmor, Nir Itzkovits, and Liad Margalit for help with experiments. This work was supported in part by grant 293438 (RUBICAN) from the European Research Council, the Dr. Miriam and Sheldon G. Adelson Medical Research Foundation, a Center of Excellence grant (1779/11) from the Israel Science Foundation, a Center of Excellence grant from the Flight Attendant Medical Research Institute (FAMRI), EC FP7 funding (INFLACARE, agreement 223151, and INSPiRE, agreement 284460), grant R37 CA40099 from the National Cancer Institute, and the Lower Saxony-Israeli Association. M.O. is incumbent of the Andre Lwoff Chair in Molecular Biology.

Received: October 1, 2015
Revised: November 24, 2015
Accepted: January 1, 2016
Published: February 4, 2016

REFERENCES

Becker, C., Fantini, M.C., and Neurath, M.F. (2006). High resolution colonoscopy in live mice. Nat. Protoc. *1*, 2900–2904.

Bedi, U., Scheel, A.H., Hennion, M., Begus-Nahrmann, Y., Rüschoff, J., and Johnsen, S.A. (2014). SUPT6H controls estrogen receptor activity and cellular differentiation by multiple epigenomic mechanisms. Oncogene *34*, 465–473.

Ben-Neriah, Y., and Karin, M. (2011). Inflammation meets cancer, with NF-κB as the matchmaker. Nat. Immunol. *12*, 715–723.

Brigati, C., Noonan, D.M., Albini, A., and Benelli, R. (2002). Tumors and inflammatory infiltrates: friends or foes? Clin. Exp. Metastasis *19*, 247–258.

Buro, L.J., Chipumuro, E., and Henriksen, M.A. (2010). Menin and RNF20 recruitment is associated with dynamic histone modifications that regulate signal transducer and activator of transcription 1 (STAT1)-activated transcription of the interferon regulatory factor 1 gene (IRF1). Epigenetics Chromatin *3*, 16.

Campos, E.I., and Reinberg, D. (2009). Histones: annotating chromatin. Annu. Rev. Genet. *43*, 559–599.

Chernikova, S.B., and Brown, J.M. (2012). R-loops and genomic instability in Bre1 (RNF20/40)-deficient cells. Cell Cycle *11*, 2980–2984.

Chernikova, S.B., Dorth, J.A., Razorenova, O.V., Game, J.C., and Brown, J.M. (2010). Deficiency in Bre1 impairs homologous recombination repair and cell cycle checkpoint response to radiation damage in mammalian cells. Radiat. Res. *174*, 558–565.

Chernikova, S.B., Razorenova, O.V., Higgins, J.P., Sishc, B.J., Nicolau, M., Dorth, J.A., Chernikova, D.A., Kwok, S., Brooks, J.D., Bailey, S.M., et al. (2012). Deficiency in mammalian histone H2B ubiquitin ligase Bre1 (Rnf20/Rnf40) leads to replication stress and chromosomal instability. Cancer Res. *72*, 2111–2119.

Clapper, M.L., Cooper, H.S., and Chang, W.C. (2007). Dextran sulfate sodium-induced colitis-associated neoplasia: a promising model for the development of chemopreventive interventions. Acta Pharmacol. Sin. *28*, 1450–1459.

Cooks, T., Pateras, I.S., Tarcic, O., Solomon, H., Schetter, A.J., Wilder, S., Lozano, G., Pikarsky, E., Forshew, T., Rosenfeld, N., et al. (2013). Mutant p53 prolongs NF-κB activation and promotes chronic inflammation and inflammation-associated colorectal cancer. Cancer Cell *23*, 634–646.

DiDonato, J.A., Mercurio, F., and Karin, M. (2012). NF-κB and the link between inflammation and cancer. Immunol. Rev. *246*, 379–400.

Ea, C.K., Hao, S., Yeo, K.S., and Baltimore, D. (2012). EHMT1 protein binds to nuclear factor-κB p50 and represses gene expression. J. Biol. Chem. *287*, 31207–31217.

Eaden, J.A., Abrams, K.R., and Mayberry, J.F. (2001). The risk of colorectal cancer in ulcerative colitis: a meta-analysis. Gut *48*, 526–535.

Fierz, B., Chatterjee, C., McGinty, R.K., Bar-Dagan, M., Raleigh, D.P., and Muir, T.W. (2011). Histone H2B ubiquitylation disrupts local and higher-order chromatin compaction. Nat. Chem. Biol. *7*, 113–119.

Fuchs, G., Shema, E., Vesterman, R., Kotler, E., Wolchinsky, Z., Wilder, S., Golomb, L., Pribluda, A., Zhang, F., Haj-Yahya, M., et al. (2012). RNF20 and USP44 regulate stem cell differentiation by modulating H2B monoubiquitylation. Mol. Cell *46*, 662–673.

Fuchs, G., Hollander, D., Voichek, Y., Ast, G., and Oren, M. (2014). Cotranscriptional histone H2B monoubiquitylation is tightly coupled with RNA polymerase II elongation rate. Genome Res. *24*, 1572–1583.

Grivennikov, S.I., Greten, F.R., and Karin, M. (2010). Immunity, inflammation, and cancer. Cell *140*, 883–899.

Hahn, M.A., Dickson, K.A., Jackson, S., Clarkson, A., Gill, A.J., and Marsh, D.J. (2012). The tumor suppressor CDC73 interacts with the ring finger proteins RNF20 and RNF40 and is required for the maintenance of histone 2B monoubiquitination. Hum. Mol. Genet. *21*, 559–568.

Hanahan, D., and Weinberg, R.A. (2011). Hallmarks of cancer: the next generation. Cell *144*, 646–674.

Hayden, M.S., and Ghosh, S. (2008). Shared principles in NF-kappaB signaling. Cell *132*, 344–362.

Figure 7. Reduced *RNF20* and *RNF40* mRNA and H2Bub1 in Human Colonic Pathologies

(A) Published microarray data (Sen and Bhaumik, 2013) was analyzed, comparing average *RNF20* and *RNF40* mRNA levels in colons of individuals with no colonic pathologies (Normal) to those of ulcerative colitis patients (UC), regardless of inflammation status. *$p < 0.05$, **$p < 0.01$. Error bars, SE.

(B) Colon samples from 25 non-specific mild chronic colitis (non-specific colitis [NSC]) patients and 19 ulcerative colitis (UC) patients were stained for H2Bub1 or total H2B. Representative cases are shown. Insets: higher magnification of dashed area. Lower magnification scale bar, 100 μm; higher magnification scale bar, 25 μm.

(C) IHC from (B) was quantified for relative H2Bub1 staining intensity in epithelium and stroma. ***$p < 0.001$. Error bars, SE.

(D) A tissue microarray from 75 human CRC patients, classified using the tumor node metastasis (TNM) system, was stained for H2Bub1 and total H2B. Scale on upper right indicates relative H2Bub1 intensity (H2Bub1/H2B). TNM stages: I, carcinoma invading the submucosa; II, carcinoma invading the muscularis propria; III, carcinoma invading through the muscularis propria into the pericolorectal tissue.

(E) Representative H2B and H2Bub1 staining of normal and cancerous human colonic tissue. Insets: higher magnification of dashed area. Lower magnification scale bar, 100 μm; higher magnification scale bar, 25 μm.

(F) Quantification of the data in (D). *$p < 0.05$, ***$p < 0.001$.

(G) *RNF20* and *RNF40* mRNA levels were compared between colorectal cancer (CRC) and corresponding normal colonic tissue, using the TCGA database (http://www.cbioportal.org/public-portal/). **$p < 0.01$. Error bars, SE.

See also Figure S7 and Table S1.

Hayden, M.S., and Ghosh, S. (2012). NF-κB, the first quarter-century: remarkable progress and outstanding questions. Genes Dev. *26*, 203–234.

Heinz, S., Romanoski, C.E., Benner, C., Allison, K.A., Kaikkonen, M.U., Orozco, L.D., and Glass, C.K. (2013). Effect of natural genetic variation on enhancer selection and function. Nature *503*, 487–492.

Hwang, W.W., Venkatasubrahmanyam, S., Ianculescu, A.G., Tong, A., Boone, C., and Madhani, H.D. (2003). A conserved RING finger protein required for histone H2B monoubiquitination and cell size control. Mol. Cell *11*, 261–266.

Jääskeläinen, T., Makkonen, H., Visakorpi, T., Kim, J., Roeder, R.G., and Palvimo, J.J. (2012). Histone H2B ubiquitin ligases RNF20 and RNF40 in androgen signaling and prostate cancer cell growth. Mol. Cell. Endocrinol. *350*, 87–98.

Kari, V., Shchebet, A., Neumann, H., and Johnsen, S.A. (2011). The H2B ubiquitin ligase RNF40 cooperates with SUPT16H to induce dynamic changes in chromatin structure during DNA double-strand break repair. Cell Cycle *10*, 3495–3504.

Karpiuk, O., Najafova, Z., Kramer, F., Hennion, M., Galonska, C., König, A., Snaidero, N., Vogel, T., Shchebet, A., Begus-Nahrmann, Y., et al. (2012). The histone H2B monoubiquitination regulatory pathway is required for differentiation of multipotent stem cells. Mol. Cell *46*, 705–713.

Katoh, H., Wang, D., Daikoku, T., Sun, H., Dey, S.K., and Dubois, R.N. (2013). CXCR2-expressing myeloid-derived suppressor cells are essential to promote colitis-associated tumorigenesis. Cancer Cell *24*, 631–644.

Kogure, M., Takawa, M., Saloura, V., Sone, K., Piao, L., Ueda, K., Ibrahim, R., Tsunoda, T., Sugiyama, M., Atomi, Y., et al. (2013). The oncogenic polycomb histone methyltransferase EZH2 methylates lysine 120 on histone H2B and competes ubiquitination. Neoplasia *15*, 1251–1261.

Koo, B.K., Stange, D.E., Sato, T., Karthaus, W., Farin, H.F., Huch, M., van Es, J.H., and Clevers, H. (2012). Controlled gene expression in primary Lgr5 organoid cultures. Nat. Methods *9*, 81–83.

Kravtsova-Ivantsiv, Y., Shomer, I., Cohen-Kaplan, V., Snijder, B., Superti-Furga, G., Gonen, H., Sommer, T., Ziv, T., Admon, A., Naroditsky, I., et al. (2015). KPC1-mediated ubiquitination and proteasomal processing of NF-κB1 p105 to p50 restricts tumor growth. Cell *161*, 333–347.

Kumar, V., and Robbins, S.L. (2007). Robbins Basic Pathology (Saunders/Elsevier).

Lawrence, T., Gilroy, D.W., Colville-Nash, P.R., and Willoughby, D.A. (2001). Possible new role for NF-kappaB in the resolution of inflammation. Nat. Med. *7*, 1291–1297.

Majno, G., and Joris, I. (2004). Cells, Tissues, and Disease: Principles of General Pathology (Oxford University Press).

Mantovani, A., Romero, P., Palucka, A.K., and Marincola, F.M. (2008). Tumour immunity: effector response to tumour and role of the microenvironment. Lancet *371*, 771–783.

Medzhitov, R. (2010). Inflammation 2010: new adventures of an old flame. Cell *140*, 771–776.

Minsky, N., Shema, E., Field, Y., Schuster, M., Segal, E., and Oren, M. (2008). Monoubiquitinated H2B is associated with the transcribed region of highly expressed genes in human cells. Nat. Cell Biol. *10*, 483–488.

Moyal, L., Lerenthal, Y., Gana-Weisz, M., Mass, G., So, S., Wang, S.Y., Eppink, B., Chung, Y.M., Shalev, G., Shema, E., et al. (2011). Requirement of ATM-dependent monoubiquitylation of histone H2B for timely repair of DNA double-strand breaks. Mol. Cell *41*, 529–542.

Myant, K.B., Cammareri, P., McGhee, E.J., Ridgway, R.A., Huels, D.J., Cordero, J.B., Schwitalla, S., Kalna, G., Ogg, E.L., Athineos, D., et al. (2013). ROS production and NF-κB activation triggered by RAC1 facilitate WNT-driven intestinal stem cell proliferation and colorectal cancer initiation. Cell Stem Cell *12*, 761–773.

Nakachi, I., Rice, J.L., Coldren, C.D., Edwards, M.G., Stearman, R.S., Glidewell, S.C., Varella-Garcia, M., Franklin, W.A., Keith, R.L., Lewis, M.T., et al. (2013). Application of SNP microarrays to the genome-wide analysis of chromosomal instability in premalignant airway lesions. Cancer Prev. Res. (Phila) *7*, 255–265.

Nakamura, K., Kato, A., Kobayashi, J., Yanagihara, H., Sakamoto, S., Oliveira, D.V., Shimada, M., Tauchi, H., Suzuki, H., Tashiro, S., et al. (2011). Regulation of homologous recombination by RNF20-dependent H2B ubiquitination. Mol. Cell *41*, 515–528.

O'Dea, E., and Hoffmann, A. (2010). The regulatory logic of the NF-kappaB signaling system. Cold Spring Harb. Perspect. Biol. *2*, a000216.

Pavri, R., Zhu, B., Li, G., Trojer, P., Mandal, S., Shilatifard, A., and Reinberg, D. (2006). Histone H2B monoubiquitination functions cooperatively with FACT to regulate elongation by RNA polymerase II. Cell *125*, 703–717.

Perkins, N.D. (2012). The diverse and complex roles of NF-κB subunits in cancer. Nat. Rev. Cancer *12*, 121–132.

Pikarsky, E., Porat, R.M., Stein, I., Abramovitch, R., Amit, S., Kasem, S., Gutkovich-Pyest, E., Urieli-Shoval, S., Galun, E., and Ben-Neriah, Y. (2004). NF-kappaB functions as a tumour promoter in inflammation-associated cancer. Nature *431*, 461–466.

Prenzel, T., Begus-Nahrmann, Y., Kramer, F., Hennion, M., Hsu, C., Gorsler, T., Hintermair, C., Eick, D., Kremmer, E., Simons, M., et al. (2011). Estrogen-dependent gene transcription in human breast cancer cells relies upon proteasome-dependent monoubiquitination of histone H2B. Cancer Res. *71*, 5739–5753.

Sato, T., Stange, D.E., Ferrante, M., Vries, R.G., Van Es, J.H., Van den Brink, S., Van Houdt, W.J., Pronk, A., Van Gorp, J., Siersema, P.D., and Clevers, H. (2011). Long-term expansion of epithelial organoids from human colon, adenoma, adenocarcinoma, and Barrett's epithelium. Gastroenterology *141*, 1762–1772.

Schetter, A.J., Heegaard, N.H., and Harris, C.C. (2010). Inflammation and cancer: interweaving microRNA, free radical, cytokine and p53 pathways. Carcinogenesis *31*, 37–49.

Schwitalla, S., Fingerle, A.A., Cammareri, P., Nebelsiek, T., Göktuna, S.I., Ziegler, P.K., Canli, O., Heijmans, J., Huels, D.J., Moreaux, G., et al. (2013). Intestinal tumorigenesis initiated by dedifferentiation and acquisition of stem-cell-like properties. Cell *152*, 25–38.

Sen, R., and Bhaumik, S.R. (2013). Transcriptional stimulatory and repressive functions of histone H2B ubiquitin ligase. Transcription *4*, 221–226.

Shema, E., Tirosh, I., Aylon, Y., Huang, J., Ye, C., Moskovits, N., Raver-Shapira, N., Minsky, N., Pirngruber, J., Tarcic, G., et al. (2008). The histone H2B-specific ubiquitin ligase RNF20/hBRE1 acts as a putative tumor suppressor through selective regulation of gene expression. Genes Dev. *22*, 2664–2676.

Shema, E., Kim, J., Roeder, R.G., and Oren, M. (2011). RNF20 inhibits TFIIS-facilitated transcriptional elongation to suppress pro-oncogenic gene expression. Mol. Cell *42*, 477–488.

Shema-Yaacoby, E., Nikolov, M., Haj-Yahya, M., Siman, P., Allemand, E., Yamaguchi, Y., Muchardt, C., Urlaub, H., Brik, A., Oren, M., and Fischle, W. (2013). Systematic identification of proteins binding to chromatin-embedded ubiquitylated H2B reveals recruitment of SWI/SNF to regulate transcription. Cell Rep. *4*, 601–608.

Shiloh, Y., Shema, E., Moyal, L., and Oren, M. (2011). RNF20-RNF40: A ubiquitin-driven link between gene expression and the DNA damage response. FEBS Lett. *585*, 2795–2802.

Tanaka, T., Kohno, H., Suzuki, R., Yamada, Y., Sugie, S., and Mori, H. (2003). A novel inflammation-related mouse colon carcinogenesis model induced by azoxymethane and dextran sodium sulfate. Cancer Sci. *94*, 965–973.

Terzić, J., Grivennikov, S., Karin, E., and Karin, M. (2010). Inflammation and colon cancer. Gastroenterology *138*, 2101–2114.e5.

Thompson, L.L., Guppy, B.J., Sawchuk, L., Davie, J.R., and McManus, K.J. (2013). Regulation of chromatin structure via histone post-translational modification and the link to carcinogenesis. Cancer Metastasis Rev. *32*, 363–376.

Ullman, T.A., and Itzkowitz, S.H. (2011). Intestinal inflammation and cancer. Gastroenterology *140*, 1807–1816.

Urasaki, Y., Heath, L., and Xu, C.W. (2012). Coupling of glucose deprivation with impaired histone H2B monoubiquitination in tumors. PLoS ONE *7*, e36775.

Wang, Z.J., Yang, J.L., Wang, Y.P., Lou, J.Y., Chen, J., Liu, C., and Guo, L.D. (2013). Decreased histone H2B monoubiquitination in malignant gastric carcinoma. World J. Gastroenterol. *19*, 8099–8107.

Ward, J.M., Yamamoto, R.S., and Brown, C.A. (1973). Pathology of intestinal neoplasms and other lesions in rats exposed to azoxymethane. J. Natl. Cancer Inst. *51*, 1029–1039.

Whitehead, R.H., VanEeden, P.E., Noble, M.D., Ataliotis, P., and Jat, P.S. (1993). Establishment of conditionally immortalized epithelial cell lines from both colon and small intestine of adult H-2Kb-tsA58 transgenic mice. Proc. Natl. Acad. Sci. USA *90*, 587–591.

Zhang, X.Y., Pfeiffer, H.K., Thorne, A.W., and McMahon, S.B. (2008). USP22, an hSAGA subunit and potential cancer stem cell marker, reverses the polycomb-catalyzed ubiquitylation of histone H2A. Cell Cycle *7*, 1522–1524.

Zhu, B., Zheng, Y., Pham, A.D., Mandal, S.S., Erdjument-Bromage, H., Tempst, P., and Reinberg, D. (2005). Monoubiquitination of human histone H2B: the factors involved and their roles in HOX gene regulation. Mol. Cell *20*, 601–611.